CFD simulations to determine wind forces acting on plants

Lustenberger Philipp[1*], Asaro Fabio[2], Arnold Kilian[1], Casartelli Ernesto[1], Luible Andreas[1]

* Corresponding author: philipp.lustenberger.01@hslu.ch
1 Lucerne University of Applied Sciences and Arts, Engineering and Architecture, Switzerland
2 AST Turbo AG, Switzerland

Abstract

Wind forces acting on plants can be calculated in CFD simulations using porous body elements. The simulations in this study showed close agreement with wind tunnel tests. Drag coefficients derived from wind-tunnel measurements can be used as input parameters for CFD simulations to estimate the drag forces on plants in wind flows. Two approaches for determining the porosity coefficient are presented and compared; both yield comparable results. Discrepancies occur primarily at low wind speeds in the range of 0-10 m/s, with deviations of up to 50%, due to the small absolute forces involved. However, this range is not relevant for the present work, which focuses on extreme wind speeds to better understand the loading of wire ropes as part of the supporting structure for climbing plants. Leaf shedding at high wind speeds is not represented in the simulation model, leading to an overestimation of wind forces in this range. To obtain conservative wind force values, a statistical adjustment of the drag coefficient is required, which reduces the remaining uncertainties. Once these adjustments are applied, the model can be used to estimate wind-induced drag forces on plants via CFD, reducing the number of physical models required.

Keywords

Green façade, CFD simulation, climbing plants, porous body, wind resistance coefficient, wind tunnel tests, wind forces

DOI

http://doi.org/10.47982/jfde.2026.334

1 INTRODUCTION

Climate change is causing temperatures in urban areas to rise, and larger cities are increasingly becoming *heat islands*. In addition to the architectural measures, greening of building surfaces is a potential solution to reduce urban temperatures (Sheweka & Mohamed, 2012). Even though façade greening is only one part of a broader strategy, with a relatively small base area, it can significantly influence a building's microclimate and help lower local environmental temperatures. This reduces the cooling demand of buildings during hot periods and provides insulation during cold periods (Bakhshoodeh et al., 2022).

Façade greening also influences the structural design of the corresponding façade systems. These systems must either be reinforced or supplemented with climbing aids for the plants. Appropriate climbing aids are particularly important for vegetated cable façades, which are often supported by brackets and cables mounted on the façade.

Such substructures and climbing aids must be able to withstand various loads. One component is the structure's own weight and the weight of the plants themselves. More critical for the design, however, are material stresses caused by temperature changes, plant growth, and wind loads (Forschungsgesellschaft Landschaftsentwicklung Landschaftsbau, 2018 (FLL)). Existing guidelines generally state that these structures must be designed to withstand such loads, but rarely specify how this should be achieved in practice. While wind loads on buildings are generally well defined, the resulting loads on the substructure of greenery exposed to wind are not well documented. The FLL *façade greening guideline* (2018) provides only an approximate method, using a reduction factor for wind loads, without addressing parameters such as rope spacing and/or wall offset.

Arnold et al. (2021a) therefore initiated the development of a new calculation approach that incorporates several parameters, including the abovementioned rope spacing and wall offset. In order to investigate the effects of these parameters, a corresponding parameter study is required. Two approaches are available: (i) wind tunnel testing and (ii) Computational Fluid Dynamics (CFD) simulations. Wind tunnel studies are complex, and plant scaling has so far only been performed on trees (Gromke, 2018). For this reason, CFD simulations are chosen for the herein described parameter study.

The CFD model used in the parameter study is developed here. It must allow a realistic calculation of the forces that the plants exert on the substructure due to wind flow, as a function of the plant growth density. To validate the simulations, the results will be compared with measurements from the wind tunnel tests by Arnold et al. (2026).

If the CFD model is successfully validated, it can be used to calculate the forces acting on plants growing around buildings. This enables replacing wind tunnel tests and avoiding the need to construct physical models. The aim is to use a parameter study with the plant model to derive a calculation guideline.

2 STATE OF THE ART

2.1 WIND FORCES ON PLANTS

Determining wind loads is essential for the design of buildings and façades, as wind is one of the main forces acting upon them. The size and shape of the structure play a decisive role in the intensity of the load. This is also reflected in the equation for calculating the drag force of an object in a flow (Bschorer & Költzsch, 2021), which applies equally to buildings and depends significantly on the velocity *u*.

$$\mathbf{F_R} = \frac{1}{2} \times \rho \times \mathbf{A} \times \mathbf{C_D} \times \mathbf{u}^2 \tag{1}$$

In Eq. (1), the size of the object is represented by the protected area *A* in the flow direction, and its shape is considered in the drag coefficient c_D.

Plants, however, respond differently to wind flow than solid, rigid objects. They can deform and adopt a more aerodynamically efficient shape. Previous studies have shown that this reconfiguration reduces the exposed surface area and, consequently, the drag force (Gosselin, 2019; Thom, 1971). Calculating the forces acting on plants in a flow is therefore significantly more complex, as both their effective frontal area and shape change continuously, i. e., as a function of the flow speed. This phenomenon has also been examined by Rudnicki et al. (2004) and Vollsinger et al. (2011). In these studies, the changing flow area made it impossible to determine a constant drag coefficient c_D, as is typically possible for rigid structures. Moreover, plants may lose leaves at high wind speeds, thereby reducing their wind resistance compared with all the foliage intact.

Based on Vogel (1989), Arnold et al. (2021a) proposed using a function, rather than a constant, to represent the drag coefficient. This function depends on wind speed and incorporates all aerodynamic changes the plants undergo during exposure to wind. In this approach, the frontal area is determined at rest and assumed constant in the subsequent calculation, while the effects of reconfiguration and leaf loss are embedded in the c_D function. This enables a simplified yet more realistic calculation of the forces acting on plants in wind currents. The data of Arnold et al. (2026) to determine the aerodynamic resistance forces–which serve as the basis for calculating the drag coefficients–were obtained in a wind tunnel on ten common climbing plant species used in façade greening. The derived c_D values provide the basis for calculating the wind resistance forces acting on climbing plants in façade greening applications.

2.2 CFD SIMULATIONS WITH PLANT BODIES

The scalability of objects investigated in wind tunnel tests is of central importance. Only with correct scaling factors can such models replicate reality as accurately as possible. This has already been achieved for tests and measurements of wind forces on trees (Chan et al., 2020; Gromke, 2018). However, climbing plants typically have a much more homogeneous leaf distribution than trees, and therefore, the results of these studies cannot be directly transferred. Since no wind tunnel tests are known for green façade plants, and there is also a lack of knowledge regarding their scaling, an alternative is to perform CFD simulations. This approach allows plants and buildings to be simulated at a 1:1 scale, eliminating the need for physical scaling.

Plants have been included in CFD simulations in various types of studies–for example, to determine evaporation performance (Plas & Paepe, 2021) or to investigate urban climate situations (Hefny Salim et al., 2015). In such studies, the plants are represented in the simulation by a substitute geometry, often modelled as a porous body with a specified permeability. This method allows simulating multiple plant configurations using the same base model by adjusting the permeability. In ANSYS CFX (2023), permeability can be defined using the following equation.

$$S_{M,i} = -\frac{\mu}{K_{Perm}} \times u_i - \frac{1}{2} \times K_{loss} \times \rho \times |u| \times u_i \quad (2)$$

A further advantage of the porous-body approach is that it avoids complex 3D meshing, since the geometry of individual leaves and stems can be simplified. For the porous-body approach to yield realistic results, the plant's aerodynamic behaviour in the flow must be accurately characterised. In particular, values for the K_{loss} factor should be derived from wind tunnel test results.

3 METHODS

3.1 POROUS BODY

The plants are assigned a defined resistance loss coefficient. In the ANSYS-CFX simulations, this is implemented using a porous-body model. The first term of the impulse loss equation (Eq. (2) is neglected, as the loss is assumed to follow a power function with dependence on the velocity (Arnold et al., 2021a). The porosity coefficient K_{loss} is a function of the drag coefficient, which was determined from the force measurements reported by Arnold et al. (2026). An isotropic momentum loss is defined for the plants, with the velocity components in the x and y directions determining the loss factor. In CFX, the momentum loss in the relevant directions can be expressed as:

$$S_{M,i} = -\frac{1}{2} \times K_{loss} \times \rho \times |u| \times u_i \quad (3)$$

The momentum loss due to porosity can also be expressed in terms of the pressure drop dP per unit length dx.

$$S_M = -\frac{d_p}{d_x} \quad (4)$$

Here, the air density ρ, the loss factor K_{loss} and the velocity u define the momentum loss.

3.2 CALCULATION METHOD

Two approaches are used to calculate the forces acting on the plants. In the first approach, the conventional drag force equation for a solid body is used at the onset.

$$F_R = \frac{1}{2} \times \rho \times A \times C_D \times u^2 \quad (5)$$

Both Arnold et al. (2021a) and Rudnicki et al. (2004) have applied this formulation to the calculation of wind forces on plants. In this case, the drag coefficient c_D can be interpreted as the resistance loss coefficient. The projected frontal area A, air density ρ, and the velocity u are included in the calculation. The projection area is subsequently treated as constant, as changes in area are implicitly accounted for within the drag coefficient.

Alternatively, the second approach by Thom (1971) can be applied.

$$F_R = \rho \times LAD \times V \times C_D \times u^2 \quad (6)$$

Here, the leaf area density *(LAD)* and the relevant volume *V* must be determined in advance, in addition to the velocity *u* and air density ρ.

Table 1 compares the two described approaches and shows that they yield different K_{loss} values when implemented in ANSYS CFX.

TABLE 1 *Comparison of calculation approaches to determine the wind forces acting on plants.*

Process variable	Arnold et al. (2021a)	Thom (1971)
Resistance force [N]	$F_R = \frac{1}{2} \times \rho \times A \times C_D \times u^2$	$F_R = \rho \times LAD \times V \times C_D \times u^2$
Drag coefficient [-]	$C_D = \frac{2 \times F_R}{\rho \times A \times u^2}$	$C_D = \frac{F_R}{\rho \times LAD \times V \times u^2}$
Loss of momentum [N*m-3]	$S_M = -\frac{dP}{dx} = -\frac{1}{2} \times K_{loss} \times \rho \times u^2$	
with	$dP = \frac{dF_R}{dA}$ $-\frac{dP}{dx} = \frac{dF_R}{dA \times d_x} = -\frac{1}{2} \times K_{loss} \times \rho \times u^2$	
CFX- input [m-1]	$K_{loss} = \frac{C_D}{dx}$	$K_{loss} = 2 \times C_D \times LAD$

3.2.1 Leaf Area Density LAD

Leaf Area Density (LAD) is used to determine the aerodynamic resistance of plants according to Thom (1971). It is defined as the ratio of half the total leaf surface area (projected area of leaves) to the volume occupied by the plant:

$$LAD = \frac{\text{half leaf surface area}}{\text{plantvolume}} \quad (7)$$

This ratio indicates plant density. For wind resistance calculations, plant density plays an important role: the more leaves and branches a plant has, the greater its exposed area to the wind. However, a linear relationship between plant density and aerodynamic resistance cannot be assumed, as at higher densities leaves shield and support each other (de Langre, 2008), which alters the flow and increases resistance.

In general, LAD varies with height, especially in plants with uneven leaf distribution, such as trees. In such cases, height-dependent LAD profiles are particularly relevant and should be incorporated into the calculation. In contrast, climbing plants tend to have a more uniform leaf distribution across their height, allowing LAD to be approximated as a constant mean value across the plant height (FIG 1).

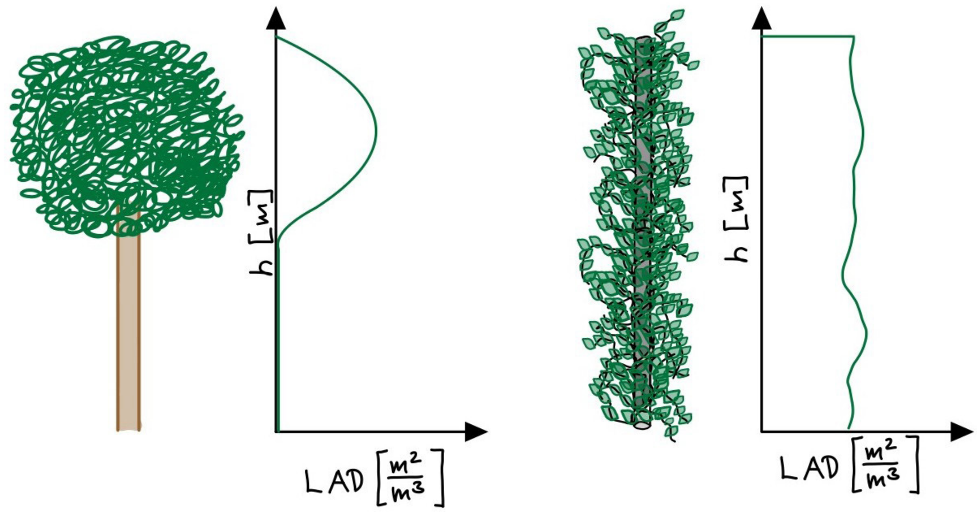

FIG. 1 Leaf Area Density (LAD) distribution of a tree in contrast to that of a climbing plant on a green façade.

4 CFD SIMULATION

4.1 OBJECTIVE

CFD simulations in ANSYS-CFX R2 (2023) are performed to replicate the results from wind tunnel tests conducted by Arnold et al. (2026). The goal is to determine plant forces from the simulation as a function of their position relative to a building. The wind tunnel tests are used to validate the plant model.

4.2 DATA BASIS

The measurement results from the wind tunnel tests on ten plants by Arnold et al. (2026) serve as the data source. FIG 2 illustrates the measured effective values and the corresponding mean value curves, where the mean curve represents a moving average over 2 m/s. From these mean value curves, the corresponding drag coefficient c_D for the two approaches outlined in Section 3.2 is calculated using:

$$C_D = \frac{2 \times F_R}{\rho \times A \times u^2} \quad \text{and} \quad C_D = \frac{2 \times F_R}{\rho \times LAD \times V \times u^2} \tag{8}$$

A power law function is subsequently fitted to these calculated c_D values to best represent the individual data points. This is done for each plant strand to enable accurate model validation.

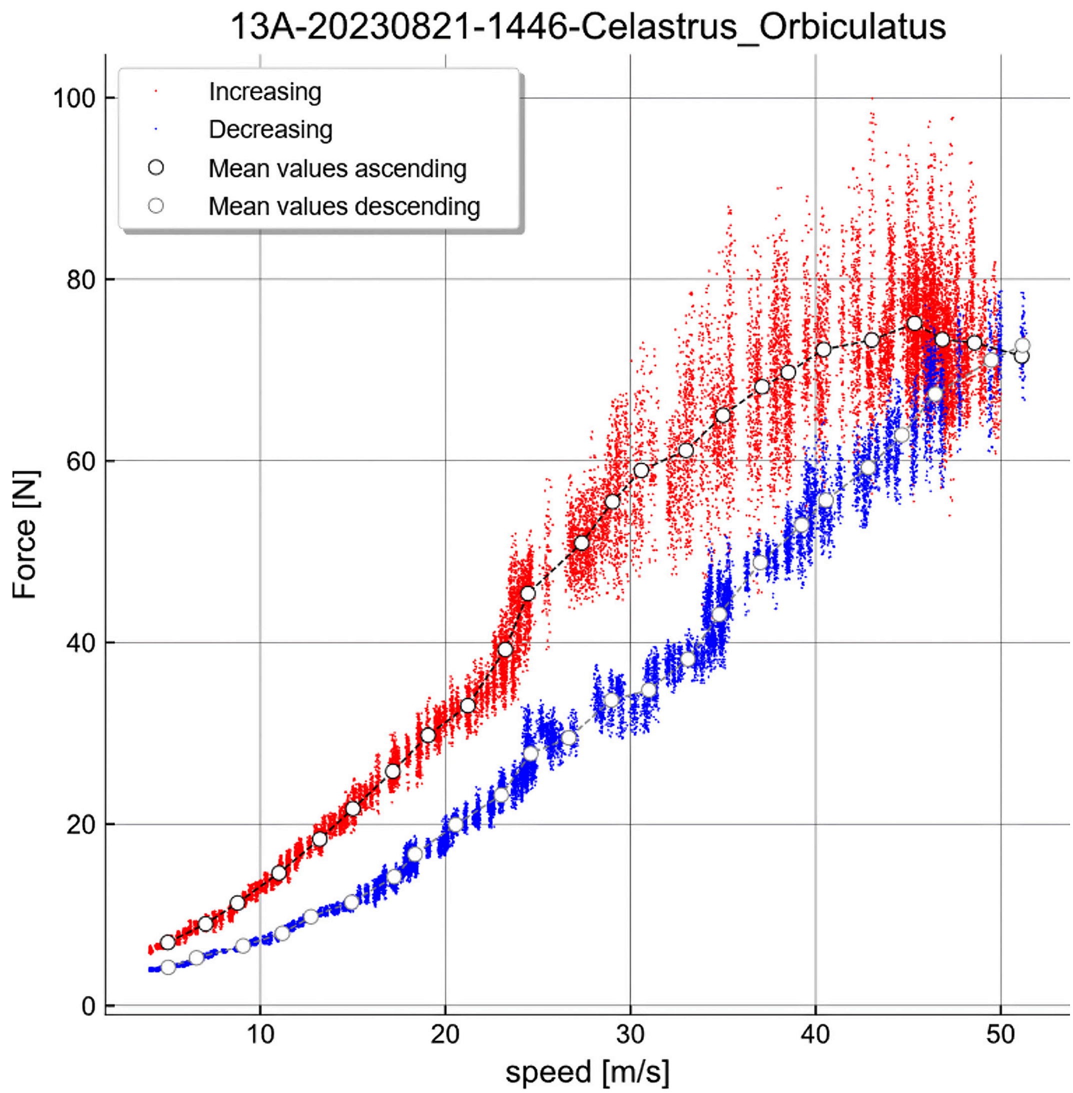

FIG. 2 Plant force as a function of wind speed in the wind tunnel tests; red: increasing speed, blue: decreasing speed (data of Arnold et al., 2026).

4.3 GEOMETRY

The calculation mesh replicates the measurement section of the wind tunnel tests but is reduced to one quarter of the tunnel cross-section of the channel using two symmetry planes, thereby reducing computational effort while maintaining close agreement with the experiments.

The plant is replaced by the porous body (red area in FIG 3). This is modelled as a continuous body. The size is variable, depending on the growth size of the plant.

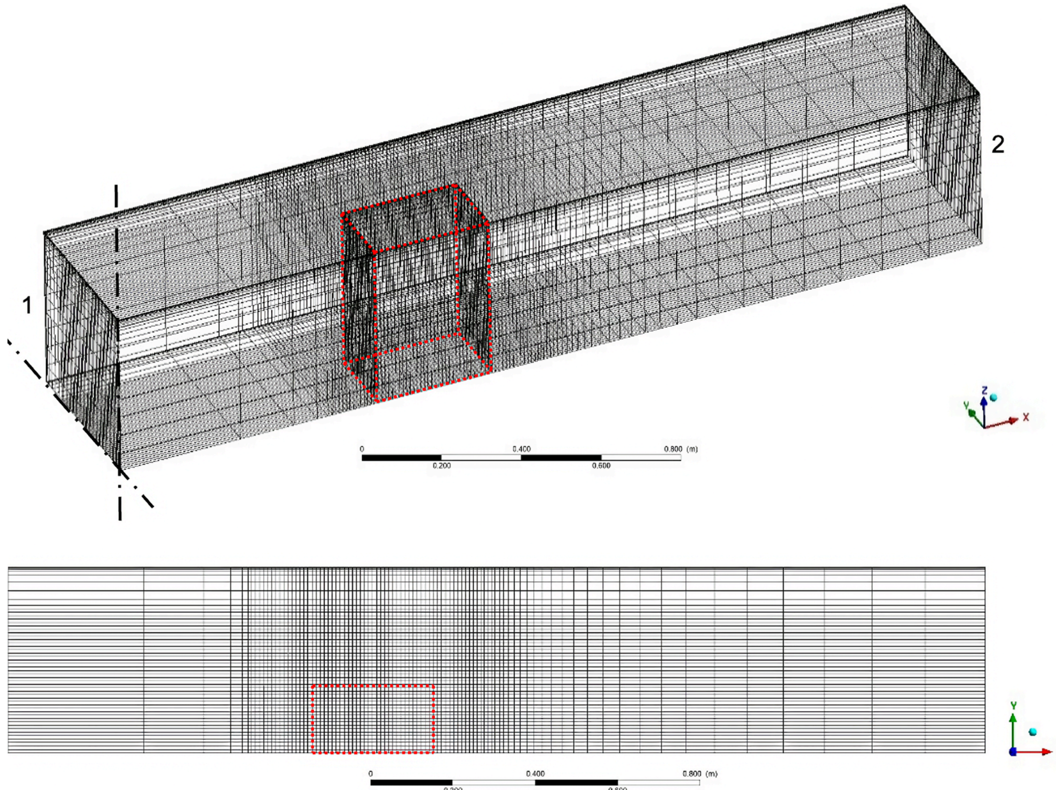

FIG. 3 Structured mesh of the wind tunnel test section (1/4 of the effective cross-section); top: 3D-view, bottom: view in z-direction.

When calculating the drag coefficient, the forces from ropes and branches are included in the drag coefficient of each plant sample. Therefore, these elements are not modelled separately but are incorporated into the plant's porous body. The mesh is structured with approximately 98,000 nodes. The plant body requires only slight refinement and is therefore coarsely meshed, whereas the wind tunnel wall has a refinement in the wall section to achieve $Y^+ \approx 100$.

4.3.1 Plant geometry

The plant diameter is derived from the projection area A_{Pr}. (FIG 4) The plant is photographed frontally and rotated by 90°, and the foliage projection area is measured. The projection area A_{Pr} is distributed over the wind tunnel height h to form a homogeneous cylinder with diameter d_{Pf} and equivalent projection area $A_{Pr.äq}$. Only regions containing foliage are included in the calculation. The equivalent diameter d_{Pf} is then used in the mesh model.

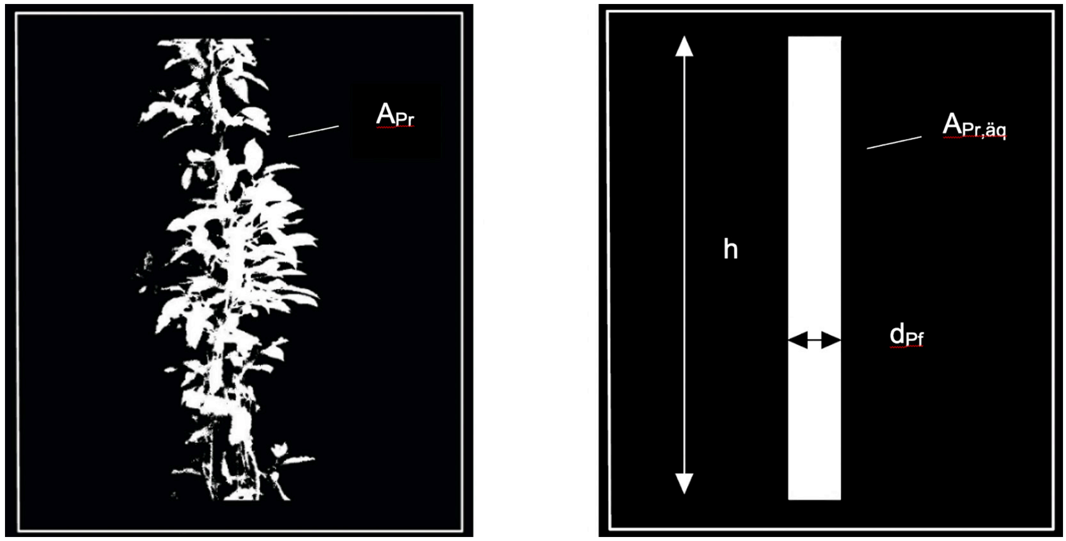

FIG. 4 Calculation of plant diameter, on the left, an effectively photographed projection surface, and on the right, an equivalent surface without air pockets.

The plant is modelled as a rectangle for two reasons. First, to enable a simpler structured mesh and second, because analysis showed that rectangular or round geometries yield negligible differences (maximum deviation of 0.6%) in calculated forces, tested for three plant diameters and K_{Loss} factors (FIG 5). This latter effect is due to the plant-induced momentum loss not generating vortices, so the geometric shape has little effect on the flow structure.

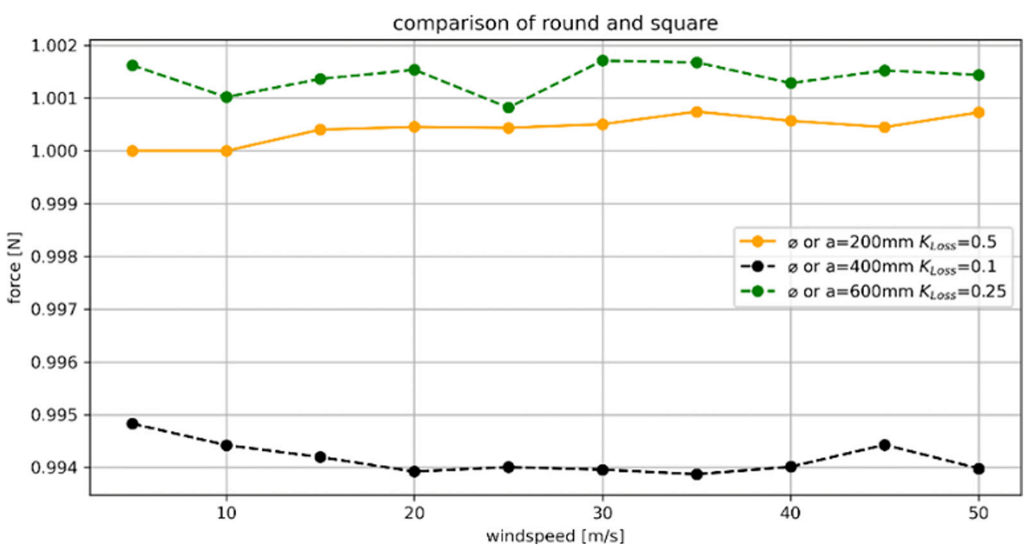

FIG. 5 Comparison of force calculation with a square (a = sidelength) and a round body.

The computational domain length in the x direction is adapted to the diameter d_{Pf}, while the domain width in the y direction is chosen such that the rectangular simulation volume corresponds to the equivalent round plant volume.

4.4 CFD-MODEL SETTINGS

In FIG 3, surface 1 is defined as the inlet with a uniform velocity profile, and surface 2 is defined as the outlet with an average static pressure condition. Inlet velocities of 5-50 m/s in 5 m/s increments are applied, with the outlet set to a relative pressure of 0 Pa.

The domain surfaces in the x- and y-directions are defined as symmetry planes, and the two outer surfaces are set as no-slip walls. The interface between air and plant is defined as a *fluid-porous interface* with a GGI mesh connection.

The porous body is defined with isotropic momentum loss as described in Section 3.1 and a volume porosity of 1, since the equivalent plant diameter is assumed to contain only plant material and no air. To achieve the desired momentum loss from Arnold et al. (2021a), the velocity magnitude *u* in Eq. (8) is calculated as

$$\mathrm{u} = \sqrt{\mathrm{u_x}^2 + \mathrm{u_y}^2} \tag{9}$$

Reflecting the assumption that plant porosity depends on the resultant velocity in the x-y plane. The input for K_{loss} follows Arnold et al. (2021a), Eq. 3.3:

$$\mathrm{C_D} \quad = \quad \mathrm{B} * \sqrt{\mathrm{u_x^2} + \mathrm{u_y^2}}^{\,-\mathrm{E}} \tag{10}$$

Forces on the plants are analysed at each speed increment within the range of 5-50 m/s. The total force acting in a given direction *i* is calculated as

$$\mathrm{F_{tot,i}} \quad = \quad \int \rho \times \mathrm{n_i} \quad \mathrm{dA} \quad + \quad \int \mathrm{v_i} \quad \mathrm{dm} \tag{11}$$

in which p is the static pressure, n_i is the face normal projected in the *i*-direction, *dA* is an infinitesimal surface element, v_i is the velocity component in the *i*-direction, and is the mass flow through an infinitesimal surface element; in other words, the first term is the pressure forces and the second term the impulse forces. The SST turbulence model is applied at the inlet with a medium turbulence intensity of 5%. *High Resolution* is selected for the advection scheme, and *First Order* is used for the turbulence numerics.

5 SIMULATION RESULTS

The simulation results are validated against the wind-tunnel data of Arnold et al. (2026). This is demonstrated using one plant sample (*Baumwuerger*) as an example, with the findings being transferable to other cases. First, the differences between the two calculation methods described in Section 3.2 are presented. FIG 6 (left) shows the calculated c_D values (points) along with their fitted c_D curves. The influence of the two approaches on the c_D curve is shown in blue and red. Both curves agree closely, with only minor deviations observed in the 20-40 m/s range.

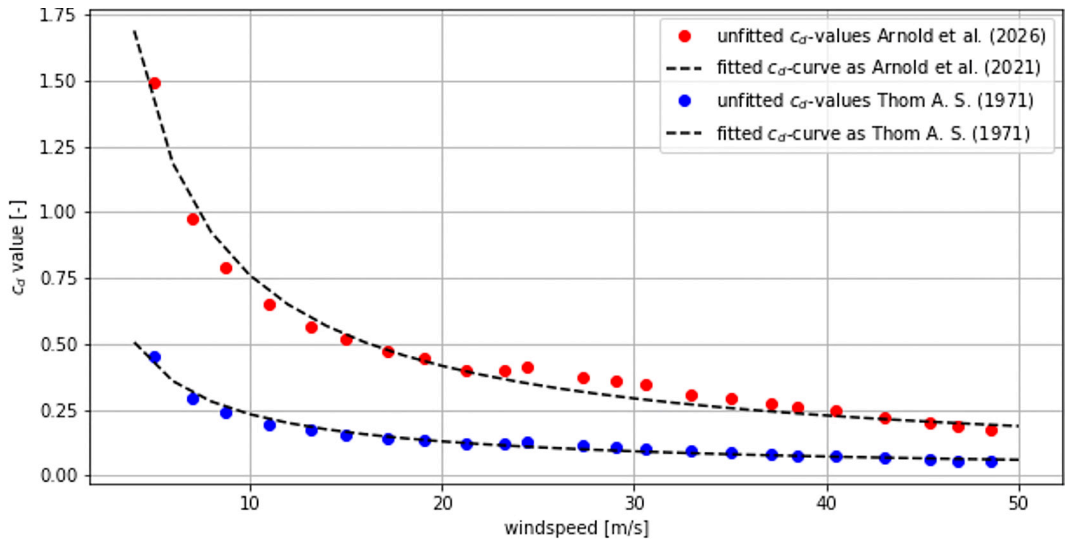

FIG. 6 Comparison of unfitted and fitted cD curves.

FIG 7 compares the simulation and wind-tunnel measurements. The two calculation approaches (green and black curves) differ by less than 3%, indicating that either method can be used. In the following analysis, the c_D-values from Arnold et al. (2026) are used. The blue (splitted c_D) curve will be explained in Section 6 and the results are discussed in Section 7.

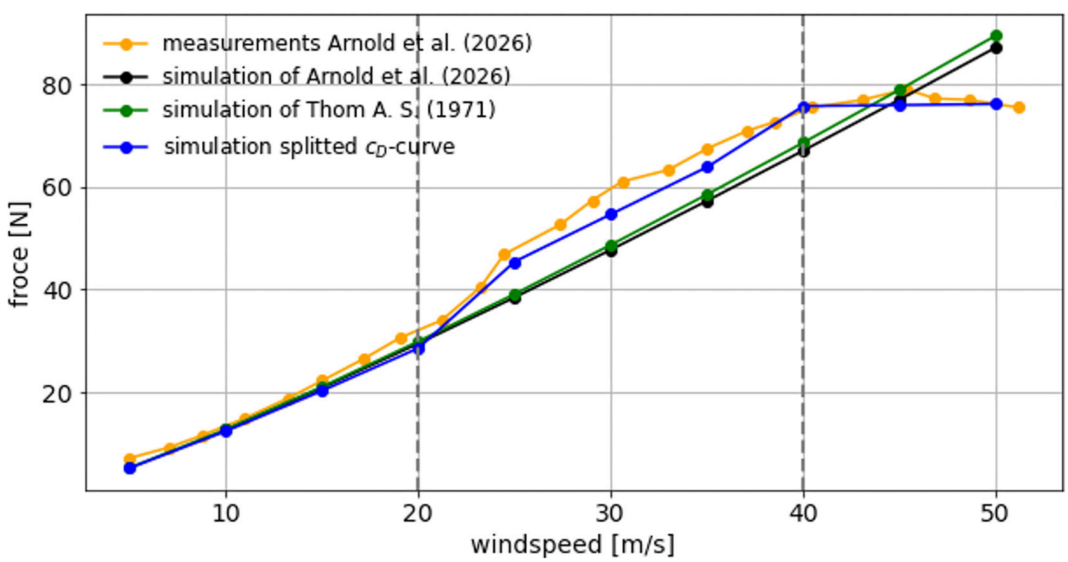

FIG. 7 Simulation results from the two calculation approaches.

FIG 8 shows that momentum loss within the porous body (blue box) causes a reduction in fluid velocity. Conversely, the constriction between the plant and the wind tunnel accelerates the flow due to a reduced cross-section. This results in different velocity distributions–and consequently pressure distribution–at the front and rear faces of the porous body, from which the aerodynamic force can be determined. Upstream of the porous body, two distinct velocity fields can be observed with minimal mixing, limited to a narrow shear zone. This occurs because the structured mesh is perfectly aligned with the flow direction.

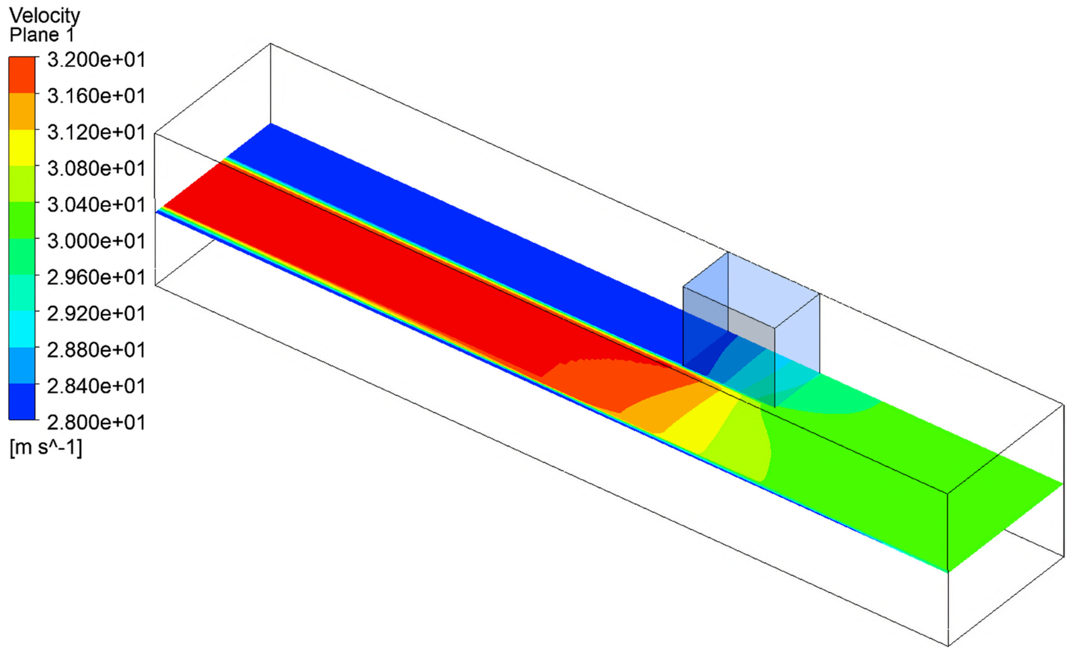

FIG. 8 Velocity field around the porous body in the wind tunnel simulation.

6 DISCUSSION

The experimental curve indicates that in the first 0-20 m/s range, the absolute simulation results closely match the measurements. The large relative percentage deviations in the 0-5 m/s range (~10%) are due to the small absolute force intensities. In the second part (20-40 m/s), the simulation underestimates the forces. This is primarily due to the fitted c_D curve presented in FIG 6, as the measured c_D values are higher than the fitted function, leading to lower simulated forces. In the third range of 40 - 50 m/s, leaf tearing occurs. The plant's aerodynamic resistance stagnates or even decreases, whereas the simulated force continues to increase. This is because the porous-body model assumes constant geometry and volume, without representing leaf loss.

The same results are shown in the evaluation of the ratios between the wind-tunnel measurement and the simulation (Boxplot of all individual plant simulations and plant measurements in FIG 9). At speeds of 0-10 m/s, there are still large uncertainties, as well as in the 20-40 m/s range. The ratios decrease at high speeds and yield more accurate simulation results near 1.0 or lower in the 40-50 m/s range (dimensioning-relevant).

An alternative approach was tested by defining three separate c_D curves–one for each velocity range (0-20, 20-40,40-50 m/s)–and repeating the simulations. This method of splitting the c_D curve produced excellent agreement with the measurements, confirming the model's mathematical correctness. However, because it would require calculating and implementing three separate c_D curves for each plant, it was used only as verification and not for general application. An adapted general function, as shown in Table 8 of Arnold et al. (2021b), is considered a possible solution.

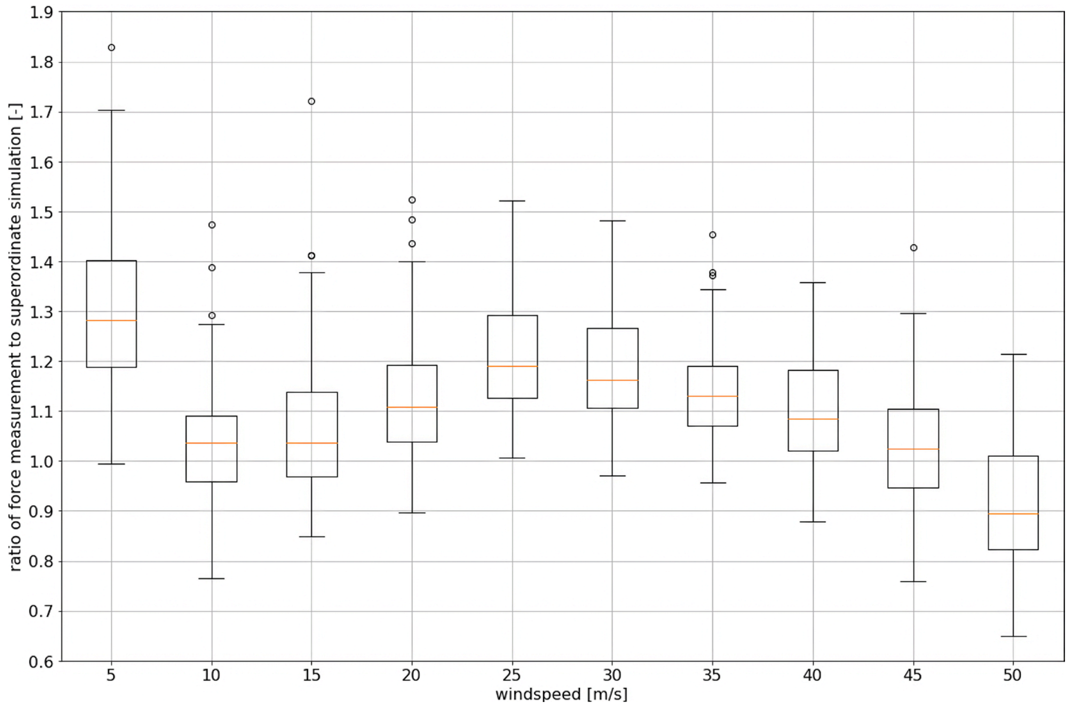

FIG. 9 Comparison of all measurements (of different plant types) of the wind tunnel tests and the simulation.

7 CONCLUSION

Plant forces can be calculated in CFD simulations using a porous-body model with relatively low modelling effort. This method achieves sufficient accuracy for the design of green façades. The three-dimensional structure of a plant can be simplified to a rectangular porous body, improving mesh quality and greatly reducing computational cost.

Both calculation approaches–the method by Thom (1971) and the conventional solid-body approach, with the c_D value from Arnold et al. (2021a)–were applied successfully, with results differing by less than 3%. Either approach can be used depending on the available plant data.

Large percentage deviations occur at low wind speeds (0-10 m/s), although the absolute values are small. For simulations focused on low wind speeds, the model should be adapted or tested under conditions optimised for that range. The results of the wind-tunnel study by Arnold et al. (2026) show the plants' behaviour at high speeds, which can affect accuracy at lower speeds. The *leaf tearing* phenomenon, as observed in the experiments, is not captured by the porous-body model. The split c_D curve approach demonstrated improved agreement with measurements but was not adopted for general use due to its complexity.

FIG 9 shows that a statistical adjustment, or a general function as in Table 8 of Arnold et al. (2021b), must be used for the calculation of conservative plant forces. This is particularly relevant if the simulation is intended to estimate the design force for the substructure.

Acknowledgements

The research project “Wind load in overgrown rope façades: CFD Study” IZCOZ0_198092 was funded by the Swiss National Science Foundation (SNSF) as part of the European Cooperation in Science & Technology (COST), Action CA17133 – Implementing nature based solutions for creating a resourceful circular city (Circular City Re.Solution). The authors gratefully acknowledge the support of SNSF, COST, and Action CA17133.

References

Ansys. (2023). *Ansys CFX* (Version 2023 R2) [Software].

Arnold, K., Fildhuth, T., Thürlemann, Y., & Luible, A. (2026). *Measurement results from wind tunnel tests on ten climbing plants for green rope facades* [Datensatz]. https://doi.org/10.5281/zenodo.18675885

Arnold, K., Gosztonyi, S., & Luible, A. (2021a). Wind Forces in Overgrown Rope Façades: Drag Coefficient Suggestion for Climbing Plants Based on Study Review. *Journal of Facade Design and Engineering*, *9*(2), 73–94. https://doi.org/10.7480/jfde.2021.2.4831

Arnold, K., Gosztonyi, S., & Luible, A. (2021b). Wind Forces in Overgrown Rope Façades: Wind Tunnel Tests on Five Climbing Plants. *Journal of Facade Design and Engineering*, *9*(2), 95–118. https://doi.org/10.7480/jfde.2021.2.4833

Bakhshoodeh, R., Ocampo, C., & Oldham, C. (2022). Evapotranspiration rates and evapotranspirative cooling of green façades under different irrigation scenarios. *Energy and Buildings*, *270*. https://doi.org/10.1016/j.enbuild.2022.112223

Bschorer, S., & Költzsch, K. (2021). *Technische Strömungslehre* (Bd. 12). Springer Fachmedien Wiesbaden GmbH.

Chan, W.-L., Eng, Y., Ge, Z., Lim, C. W. C., Gobeawan, L., Poh, H. J., Wise, D. J., Burcham, D. C., Lee, D., Cui, Y., & Khoo, B. C. (2020). Wind Loading on Scaled Down Fractal Tree Models of Major Urban Tree Species in Singapore. *Forests*, *11*(8), Artikel 8. https://doi.org/10.3390/f11080803

de Langre, E. (2008). Effects of Wind on Plants. *Annual Review of Fluid Mechanics*, *40*(1), 141–168. https://doi.org/10.1146/annurev.fluid.40.111406.102135

Forschungsgesellschaft Landschaftsentwicklung Landschaftsbau. (2018). *Fassadenbegrünungsrichtlinien—Richtlinien für die Planung, Bau und Instandhaltung von Fassadenbegrünungen*. https://shop.fll.de/de/fassadenbegruenungsrichtlinien-richtlinien-fuer-die-planung-bau-und-instandhaltung-von-fassadenbegruenungen-2018-downloadversion.html

Gosselin, F. P. (2019). Mechanics of a plant in fluid flow. *Journal of Experimental Botany*, *70*(14), 3533–3548. https://doi.org/10.1093/jxb/erz288

Gromke, C. (2018). Wind tunnel model of the forest and its Reynolds number sensitivity. *Journal of Wind Engineering and Industrial Aerodynamics*, *175*, 53–64. https://doi.org/10.1016/j.jweia.2018.01.036

Hefny Salim, M., Heinke Schlünzen, K., & Grawe, D. (2015). Including trees in the numerical simulations of the wind flow in urban areas: Should we care? *Journal of Wind Engineering and Industrial Aerodynamics, Selected papers from the 6th International Symposium on Computational Wind Engineering CWE 2014*, *144*, 84–95. https://doi.org/10.1016/j.jweia.2015.05.004

Plas, W., & Paepe, M. D. (2021). Modelling plant transpiration and leaf climate using CFD. *Journal of Physics: Conference Series*. https://doi.org/10.1088/1742-6596/2116/1/012076

Rudnicki, M., Mitchell, S. J., & Novak, M. D. (2004). Wind tunnel measurements of crown streamlining and drag relationships for three conifer species. *Canadian Journal of Forest Research*, *34*(3), 666–676. https://doi.org/10.1139/x03-233

Sheweka, S. M., & Mohamed, N. M. (2012). Green Facades as a New Sustainable Approach Towards Climate Change. *Energy Procedia, Terragreen 2012: Clean Energy Solutions for Sustainable Environment (CESSE)*, *18*, 507–520. https://doi.org/10.1016/j.egypro.2012.05.062

Thom, A. S. (1971). Momentum Absorption by Vegetation. *Quarterly Journal of the Royal Meteorological Society*, *97*(414), 414–428.

Vogel, S. (1989). Drag and Reconfiguration of Broad Leaves in High Winds. *Journal of Experimental Botany*, *40*(8), 941–948. https://doi.org/10.1093/jxb/40.8.941

Vollsinger, S., Mitchell, S., Byrne, K., Novak, M., & Rudnicki, M. (2011). Wind tunnel measurements of crown streamlining and drag relationships for several hardwood species. *Canadian Journal of Forest Research*, *35*, 1238–1249. https://doi.org/10.1139/x05-051